

Magnetic properties of monolayer, multilayer, and bulk CrTe₂

A. A. Katanin^{1,2} and E. M. Agapov^{3,4}

¹*Center for Photonics and 2D Materials, Moscow Institute of Physics and Technology,
Institutsky lane 9, Dolgoprudny, 141700, Moscow region, Russia*

²*M. N. Mikheev Institute of Metal Physics of the Ural Branch of the Russian Academy of Sciences,
S. Kovalevskaya Street 18, 620990 Yekaterinburg, Russia*

³*Ludwig-Maximilians-Universität München, Geschwister-Scholl-Platz 1, Munich, Germany*

⁴*Technical University of Munich, School of Natural Sciences, Arcisstraße 21, Munich, Germany*
(Dated: September 11, 2024)

We investigate magnetic properties of CrTe₂ within the density functional theory (DFT) approach in ferromagnetic phase and combination of DFT and dynamical mean field theory (DFT+DMFT) approach in paramagnetic phase. We show that few layer CrTe₂ possesses well formed local magnetic moments. In the single layer CrTe₂ we find antiferromagnetic exchange with 120° antiferromagnetic structure most preferable. In the bilayer and trilayer systems electronic correlations in DFT+DMFT approach yield ferromagnetic exchange interaction within each layer, but the interaction between the layers is antiferromagnetic, such that alternation of the direction of magnetization of the layers is expected. In bulk CrTe₂ we find the tendency to ferromagnetic order at low temperature, but with increase of temperature antiferromagnetic correlations between the layers dominate. Determination of the critical number of layers at which the interlayer antiferromagnetic order changes to the ferromagnetic one, requires consideration of the non-local Coulomb interactions.

I. INTRODUCTION

Atomically thin two-dimensional (2D) van der Waals (vdW) materials have attracted significant attention over the past decade due to their exceptional properties [1–6]. In particular, they can possess large magnetic moments, substantial Curie temperature, comparable to room temperature, and strong anisotropy. With these properties, 2D magnetic materials are promising for using in the fields of spintronics [2] and memory storage devices [5]. Currently, many 2D ferromagnetic (FM) materials have been reported; however, a key challenge remains: achieving ferromagnetism at room temperature. According to the Mermin–Wagner theorem, long-range magnetic order cannot exist in two dimensions in isotropic systems at finite temperatures due to thermal fluctuations. However, it is possible to circumvent this limitation by magnetic anisotropy.

Recently, chromium ditelluride CrTe₂ has been suggested to exhibit ferromagnetic order even up to room temperature, making it an attractive candidate for further research in this field. Bulk CrTe₂ was shown [7] to possess FM order with $T_C = 330$ K and in-plane magnetic anisotropy. Recent years several groups obtained thin CrTe₂ flakes via mechanical exfoliation [8–10], chemical vapor deposition [11] and molecular beam epitaxy [12–15], showing stable FM order with $T_C \sim 200$ K. While thick films were shown to have an in-plane magnetic anisotropy [8–10], the films thinner 10 monolayers show the out-of-plane magnetic anisotropy [11–13]. The authors of Refs. [11, 13, 14, 16, 17] succeeded fabricating monolayer devices. At the same time, the results of the magnetic state of monolayers remain controversial. Experimentally both, FM [11, 13, 14] and zigzag antiferromagnetic (AFM-zz) [17] states were reported.

Theoretically, the density functional theory (DFT) ap-

proach was used to study various magnetic orders and exchange interactions in CrTe₂. In particular, FM [18–22], AFM [23–25], charge density wave [26] and incommensurate [25] states were considered as possible candidates in single layer CrTe₂. It was suggested in Ref. [23] that the intralayer coupling of 2 to 4 layer CrTe₂ is still antiferromagnetic, similar to that of monolayer CrTe₂, and changes to ferromagnetic for larger number of layers. At the same time, the interlayer exchange interaction was also found to change from AFM to FM between 4 and 5 layers. The change of the magnetic orders was related by authors of Ref. [23] to the change of lattice constants from single-layer to the bulk. It was suggested in Ref. [22, 23, 27, 28] that relatively small strain can cause transition from AFM-zz to FM what explains experimental data and theoretical discrepancies.

At the same time, Cr is an open almost half filled d shell metal and possesses strong correlations. Zhu et. al. [28] showed that the effect of Hubbard interaction can be essential for the choice of magnetic phase in CrTe₂. Also, the authors of Ref. [23] emphasized that the on-site Coulomb repulsion changes the interlayer coupling to AFM even in the bulk; important role of the Coulomb repulsion for bilayer systems was also discussed in Ref. [29]. Previous theoretical works [18, 19, 21, 27, 29] used DFT+ U approach to account for correlation effects. However, for metallic systems this approach may be insufficient. To treat the effect of correlations we consider in the present study the DFT+DMFT approach. We use recently proposed method of evaluation of exchange interactions in paramagnetic phase [30] to obtain unbiased estimate of exchange interactions, which account for correlation effects and consider also their temperature dependence. We compare the obtained results to those from DFT approach.

The plan of the paper is the following. In Section II we

describe used methods for magnetic properties of CrTe₂ investigation. In Section III we present results for temperature and momentum dependence of magnetic susceptibilities, exchange interactions for monolayer, followed by study of bilayer and trilayer systems. In the end of the Section we consider bulk system to understand the limit of large number of layers. Finally, in Sect. IV we present Conclusions.

II. METHODS AND PARAMETERS

To obtain band structures we use DFT approach implemented in the Quantum Espresso [31] package with ultrasoft pseudo-potentials from SSSP PBEsol Precision library [32], supplemented by the maximally localized symmetry-adapted [33] Wannier projection onto 3d states of Cr and 5p states of Te performed within Wannier90 package [34].

For the bulk CrTe₂ we choose the experimental lattice parameters [7] $a_{\text{bulk}} = 3.7887$ Å, $c_{\text{bulk}} = 6.0955$ Å. The momentum grid $18 \times 18 \times 18$ was chosen. For the single-layer CrTe₂ we choose the lattice parameter of Ref. [25] $a = 3.71$ Å and consider interlayer spacing $c = 20$ Å to avoid overlap of the orbitals between the layers; the momentum grid $20 \times 20 \times 1$ was chosen. The vertical position of Te atoms was relaxed, and constituted the distance 1.55 Å for the bulk and 1.62 Å for the single-layer system from the Cr plane. For the bilayer (trilayer) CrTe₂ we choose the lattice parameter of Ref. [19] $a = 3.76$ Å ($a = a_{\text{bulk}}$) and consider the unit cell of the vertical size $c = 40$ Å (60 Å). The interlayer spacing was chosen equal to c_{bulk} , Ref. [10]. The relaxed vertical position of Te atoms constituted the distance 1.61 Å (1.56 Å) from the Cr plane for the outer (inner) atoms for the bilayer system and 1.58 Å (1.55 Å) for the trilayer system. The momentum grid was chosen $24 \times 24 \times 1$.

The DMFT calculations of the self-energies, non-uniform susceptibilities and exchange interactions were performed within the continuous-time Quantum Monte Carlo (CT-QMC) method of the solution of impurity problem [35], realized in the iQIST software [36]. In DMFT calculation we consider the basis, which diagonalises crystal field, and use the density-density interaction matrix, parameterized by Slater parameters F^0 , F^2 , and F^4 , expressed through Hubbard U and Hund J_H interaction parameters according to $F^0 = U$ and $(F^2 + F^4)/14 = J_H$, $F^2/F^4 \simeq 0.63$ (see Ref. 37). The Coulomb interaction parameters were chosen $U = 2.8$ eV, $J_H = 0.9$ eV. We use a double-counting correction in the around mean-field form [38].

To determine the exchange interactions we consider the effective Heisenberg model with the Hamiltonian $H = -(1/2) \sum_{\mathbf{q}, rr'} J_{\mathbf{q}}^{rr'} \mathbf{S}_\mathbf{q}^r \mathbf{S}_{-\mathbf{q}}^{r'}$, $\mathbf{S}_\mathbf{q}^r$ is the Fourier transform of static operators \mathbf{S}_{ir} at the site r of cell i , where the orbital-summed on-site static spin operators $\mathbf{S}_{ir} = \sum_m \mathbf{S}_{irm}$. The exchange interactions

in DFT were estimated by magnetic force theorem (MFT) approach [39–41] using electron Green's functions, calculated in Wannier basis $G_{rr',\sigma}^{mm'}(\mathbf{k}, i\nu_n) = [(i\nu_n + \mu)I - H_{\mathbf{k},\sigma}^{rm,rm'}]_{rm,rm'}^{-1}$, where $H_{\mathbf{k},\sigma}^{rm,rm'}$ is the Wannier Hamiltonian, I is the identity matrix, and the inversion is performed in the site- and orbital space,

$$J_{\mathbf{q}}^{rr'} = -\frac{2T}{m_r m_{r'}} \sum_{\mathbf{k}, i\nu_n} \text{Tr} \left[\Delta_r \tilde{G}_{rr',\downarrow}(\mathbf{k} + \mathbf{q}, i\nu_n) \right. \\ \left. \times \Delta_{r'} \tilde{G}_{r'r',\uparrow}(\mathbf{k}, i\nu_n) \right] \quad (1)$$

where $\Delta_{r'}^{mm'} = \sum_{\mathbf{k}} (H_{\mathbf{k},\uparrow}^{rm,rm'} - H_{\mathbf{k},\downarrow}^{rm,rm'})$ is spin splitting and $\tilde{G}_{rr',\sigma}^{mm'}(\mathbf{k}, i\nu_n) = G_{rr',\sigma}^{mm'}(\mathbf{k}, i\nu_n) - \sum_{\mathbf{k}'} G_{rr',\sigma}^{mm'}(\mathbf{k}', i\nu_n)$, the trace is taken over orbital indexes, and m_r is the magnetic moment at the r -th atom (in units of Bohr magneton μ_B). For calculations we have used 200 Matsubara fermionic frequencies.

The exchange interactions in paramagnetic phase in DMFT were calculated from the orbital-summed susceptibilities as [30, 42, 43] $\hat{J}_{\mathbf{q}} = \hat{\chi}_{\text{loc}}^{-1} - \hat{\chi}_{\mathbf{q}}^{-1}$, where hats stand for matrices $n \times n$ in the atom number in the unit cell, $\chi_{\mathbf{q}}^{rr'} = -\langle \langle S_{\mathbf{q}}^{r,z} | S_{-\mathbf{q}}^{r',z} \rangle \rangle_{\omega=0}$ is the matrix of the non-local static longitudinal susceptibilities, containing local vertex corrections, and obtained from the respective Bethe-Salpeter equation [44, 45] with account of 60-80 fermionic Matsubara frequencies, including also corrections to finite frequency box [45], $\chi_{\text{loc}}^{rr'} = -\langle \langle S_i^{r,z} | S_i^{r,z} \rangle \rangle_{\omega=0} \delta_{rr'}$ is the diagonal matrix of local spin susceptibilities. The exchange interaction in real space is obtained by performing Fourier transform of $J_{\mathbf{q}}$.

III. RESULTS

The DFT band structure of single-layer CrTe₂ in the paramagnetic state is shown in Fig. 1. In an agreement

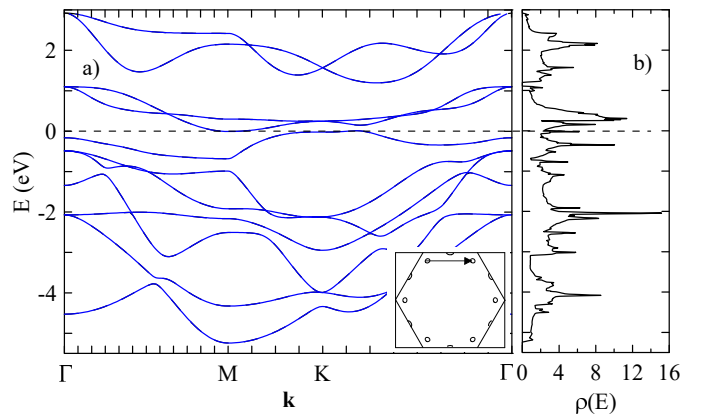


FIG. 1. (Color online) Band structure (a) and DFT density of states (b) of the single-layer CrTe₂ in paramagnetic phase. The inset in (a) shows the DFT Fermi surface; the arrow shows the nesting vector which is close to $\mathbf{Q}_K = \overline{\Gamma K}$.

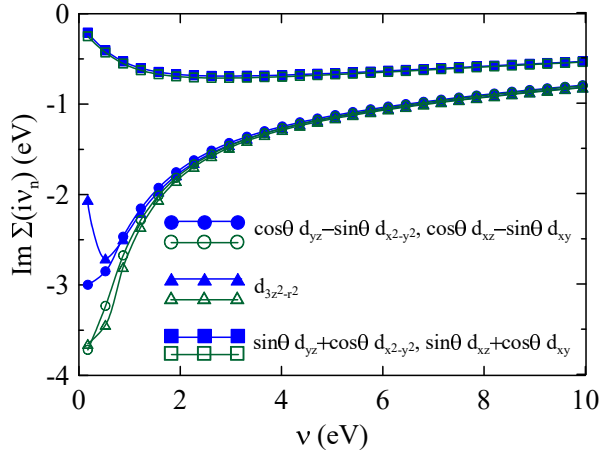


FIG. 2. Imaginary part of the self-energy of various orbital combinations of single-layer (blue solid symbols) and bilayer (green open symbols) CrTe₂ at the imaginary frequency axis in DFT+DMFT approach at $\beta = 18 \text{ eV}^{-1}$.

with the earlier study [10], the density of states contains weak peak at the Fermi level, which originates from the flat parts of the dispersion. The corresponding Fermi surface contains only small pockets near K , K' , and M points of the Brillouin zone.

The filling of d-orbitals of chromium, obtained in DFT+DMFT calculations for the single layer compound CrTe₂, is $n_{\text{Cr}} = 4.83$, and, therefore, sufficiently close to half filling, which provides rather strong correlation effects. In Fig. 2 we show imaginary parts of the electronic self-energy for combinations of orbitals, which diagonalize crystal field (the rotation angle $\theta \simeq \pi/3$). One can see that the for some of the states (those which are close to the Fermi level) the damping of electronic excitations is particularly large, and the self-energy for some of the combinations has a non-quasiparticle form with $\partial \text{Im} \Sigma / \partial \nu > 0$.

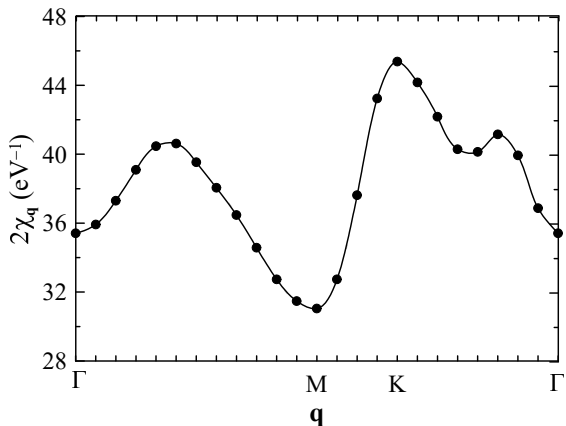


FIG. 3. Momentum dependence of the orbital-summed susceptibility of the single-layer CrTe₂ in DFT+DMFT approach at $\beta = 7 \text{ eV}^{-1}$.

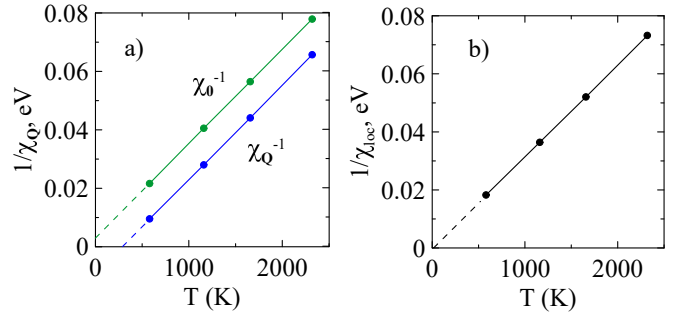


FIG. 4. (Color online) Inverse uniform and staggered, $\mathbf{Q} = \mathbf{Q}_K$ (a) and local (b) spin susceptibility of the single-layer CrTe₂ in DFT+DMFT approach. Dashed lines show extrapolation to the low-temperature region.

The obtained magnetic susceptibility at $\beta = 7 \text{ eV}^{-1}$ is rather large (see Fig. 3) and has a maximum at the wave vector $\mathbf{Q}_K = (4\pi, 0)/(3a)$, corresponding to the tendency to the 120° incommensurate magnetic order. Despite strong incoherence of electronic excitations, this tendency is likely related to the nesting of the pockets of the Brillouin zone, as shown in the inset of Fig. 1a. The susceptibility does not show even local maximum near the Γ point, which implies an absence of pronounced tendency towards ferromagnetic order.

The temperature dependence of the inverse uniform and staggered magnetic susceptibilities is shown in Fig. 4. The corresponding DMFT Neel temperature, obtained by the extrapolation of the inverse staggered susceptibility, $T_N^{\text{DMFT}, 1\text{-layer}} \simeq 300 \text{ K}$. At the same time, the inverse uniform susceptibility is extrapolated to the small negative Weiss temperature, showing absence of the ferromagnetic order, in agreement with the conclusion from the momentum dependence of the non-uniform susceptibility. The inverse local susceptibility (see Fig. 4b) is almost linear in temperature, showing well formed local magnetic moments with negligibly small Kondo temperature, estimated as an offset of linear extrapolation from zero. The local magnetic moment, obtained from the slope of the local (staggered) susceptibility $\mu_{\text{loc}}^2 = 32.4\mu_B^2$ ($\mu^2 = 31.7\mu_B^2$), corresponding to the local effective spin $S_{\text{eff}} \simeq 2.4$ defined by $\mu^2 = (g\mu_B)^2 S_{\text{eff}}(S_{\text{eff}} + 1)$, $g = 2$ is the spin g -factor.

Magnetic exchange interactions of single-layer CrTe₂ at $\beta = 20 \text{ eV}^{-1}$ are shown in Fig. 5. The maximum of the exchange interaction in both DFT and DFT+DMFT approaches is also found at the wave vector \mathbf{Q}_K , which corresponds to the 120° antiferromagnetic order. Locally FM order is stable in DFT due to local maximum at the Γ point with $J_0 > 0$ and unstable in DMFT, but in both cases Γ point is not a global maximum, which corresponds to an instability of ferromagnetism in Heisenberg model. We find the peak of exchange interaction $J_{\mathbf{q}}$ at $\mathbf{q} = \mathbf{Q}_K$ in DFT approach sharply increases with decrease of temperature (see the results of $\beta = 10 \text{ eV}^{-1}$ in Fig. 5 for comparison), due to nesting of the Fermi surface pockets with the wave vector close to

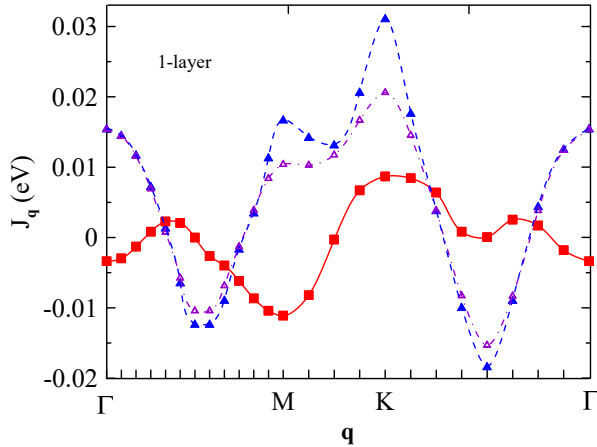


FIG. 5. (Color online) Exchange interaction in single-layer CrTe₂ at $\beta = 20 \text{ eV}^{-1}$. Red solid line (squares) corresponds to DFT+DMFT approach in paramagnetic phase, blue dashed line (filled triangles) is the result of the DFT approach in FM phase. For comparison, the result of DFT approach at $\beta = 10 \text{ eV}^{-1}$ is shown by dot-dashed violet line with open triangles

\mathbf{Q}_K (see Appendix A). At the same time, the exchange interactions in DFT+DMFT approach are quite weakly temperature dependent, because of the damping of electronic excitations. We also note that in the ferromagnetic ordered phase of DFT we obtain magnetic moment of chromium sites $\mathbf{m} = 2.86\mu_B$, which corresponds to effective spin $S_{\text{ord}} = \mathbf{m}/(g\mu_B) = 1.48$. This reflects different spin state of chromium in the ferro- and paramagnetic phase: while the chromium occupation is close in two approaches ($n_{\text{Cr}} = 4.67$ in DFT), the effective spin difference $\Delta S = S_{\text{eff}} - S_{\text{ord}} \simeq 1$ corresponds to only partial magnetization of orbital states. In particular, we find strongest magnetization contribution $0.8\mu_B/\text{f.u.}$ from $d_{3z^2-r^2}$ state and weakest contribution $0.4\mu_B/\text{f.u.}$ from each of the $d_{xz,yz}$ states.

We also used alternative method to obtain exchange interactions, based on comparison of energies of various spin configurations [18], see Appendix B. The comparison of the obtained exchange interactions is presented in Table I. All DFT approaches, except Ref. [18] yield the same signs of nearest- and next-nearest neighbor ex-

Method	J_1	J_2	J_3
DFT Energies, this work	-2.03	1.53	-0.43
DFT MFT, this work	-1.51	3.52	2.06
DMFT, this work	0.08	1.16	-1.34
DFT Energies [18]	5.20	0.94	
all-electron KKR-GF [25]	-3.19	2.37	1.18

TABLE I. Exchange interactions (in meV) in monolayer CrTe₂ for nearest (J_1), next nearest (J_2) and next to next nearest (J_3) neighbours. DFT MFT and DMFT exchange interactions are calculated at $\beta = 20 \text{ eV}^{-1}$.

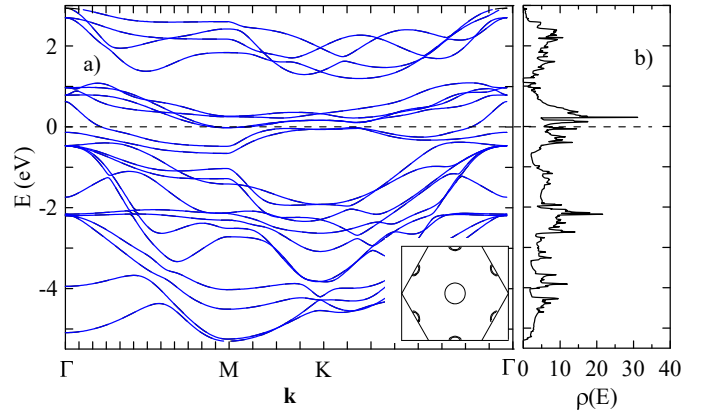


FIG. 6. (Color online) Band structure (a) and DFT density of states (b) of the bilayer CrTe₂ in paramagnetic phase. The inset in (a) shows the DFT Fermi surface.

change interactions, with different magnitude. In particular, the nearest neighbour exchange interaction is negative (except Ref. [18]) showing the tendency to antiferromagnetism. We find the sAFM-zz configuration in DFT approach 10 meV/f.u. lower than FM. At the same time, in DMFT approach we find weak ferromagnetic nearest

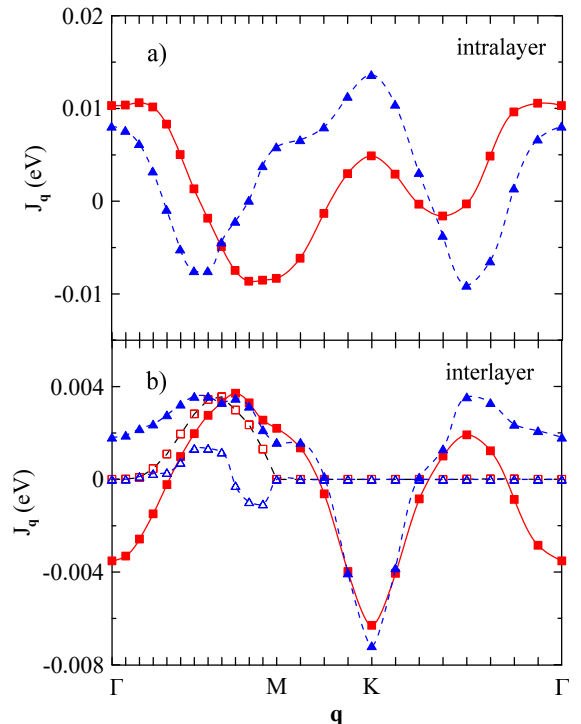


FIG. 7. (Color online) Exchange interaction in bilayer CrTe₂ at $\beta = 18 \text{ eV}^{-1}$ (a) between the atoms of the same layer $J_{\mathbf{q}}^{11}$ and (b) between the atoms of different layers $J_{\mathbf{q}}^{12}$. Red solid line (squares) corresponds to DFT+DMFT approach in paramagnetic phase, blue dashed line (triangles) is the result of the DFT approach in FM phase. Full (open) symbols in (b) correspond to the real (imaginary) part.

neighbor exchange interaction, and the tendency to anti-ferromagnetism originates from the next to next nearest neighbors and further interactions.

To study effect of interlayer coupling we consider bilayer and trilayer CrTe_2 . The band structure of bilayer CrTe_2 in paramagnetic phase is shown in Fig. 6. One can see that due to bilayer splitting the central sheet of the Fermi surface appears at the Γ point. The electronic self-energies are shown in Fig. 2. One can see that the electronic damping for the bilayer system is even larger than for the single-layer one, and non-quasiparticle form of the self-energy is also more pronounced.

We consider the interaction between the atoms of the same Cr plane (intralayer part), $J_{\mathbf{q}}^{rr}$ and the interplane interaction $J_{\mathbf{q}}^{rr'}$ with $r \neq r'$. From the momentum dependence of intralayer exchange interactions $J_{\mathbf{q}}^{11} = J_{\mathbf{q}}^{22}$ (see Fig. 7a) one can see that additional sheet of the Fermi surface strongly affects exchange interactions: the intralayer interaction becomes maximal near Γ point of the Brillouin zone, while the height of the local maximum at the K point decreases in comparison to the single-layer system. The obtained maximum of the intralayer exchange interaction can be contrasted to the results of DFT approach of the present study (shown by dashed line in Fig. 7a) and earlier DFT study [28], where the antiferromagnetic ground state was obtained. In case of bilayer system, both DFT and DFT+DMFT results for exchange interactions are weakly temperature dependent because of the absence of nesting and shift of the peak of the density of states from the Fermi level.

To demonstrate the possibility of intralayer ferromagnetic order in the bilayer CrTe_2 , we also show the temperature dependence of the inverse uniform intralayer susceptibility $(\chi_{\mathbf{q}=0}^{11,22})^{-1}$ in Fig. 8. One can see that in contrast to single-layer CrTe_2 the inverse intralayer susceptibility vanishes at the DMFT Curie temperature

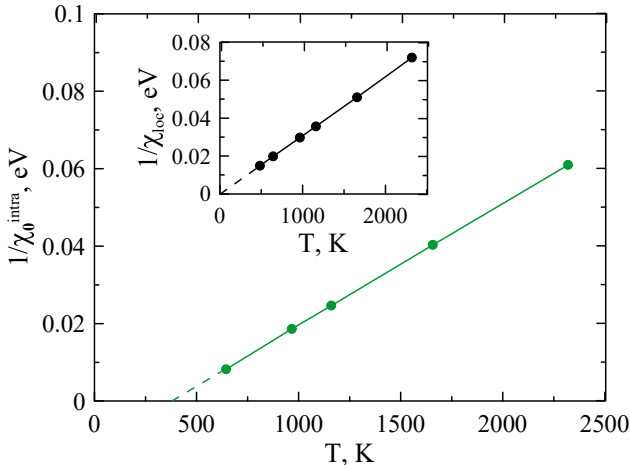


FIG. 8. (Color online) Inverse uniform intralayer susceptibility (main plot) and local susceptibility (inset) of the bilayer CrTe_2 in DFT+DMFT approach. Dashed lines show extrapolation to the low-temperature region.

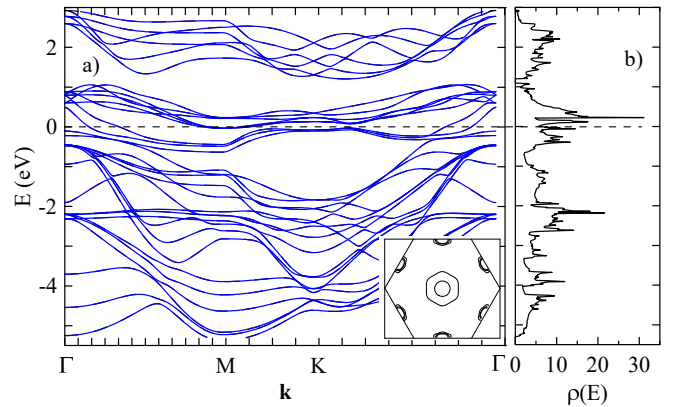


FIG. 9. (Color online) Band structure (a) and DFT density of states (b) of the trilayer CrTe_2 in paramagnetic phase. The inset in (a) shows the DFT Fermi surface.

$T_C^{\text{DMFT,2-layer}} \simeq 400K$. Similarly to the single-layer system, this DMFT Curie temperature does not determine the true Curie temperature of the system, but rather the scale of the onset of strong ferromagnetic correlations. The temperature dependence of the local magnetic susceptibility (see the inset of Fig. 8) is similar to the single-layer case, and it is characterized by the magnetic moment $\mu_{\text{loc}}^2 = 33.1\mu_B^2$, which is also close to that for the single-layer compound. Therefore the strong change of the non-local properties when passing from single- to bilayer CrTe_2 almost does not affect the local properties.

The interlayer exchange interaction $J_{\mathbf{q}}^{12} = (J_{\mathbf{q}}^{21})^*$ of the bilayer system is negative at the Γ -point (see Fig. 7b), showing the tendency to opposite orientation of spins in the layers, similarly to the previous DFT+ U studies [23, 29], while the DFT approach yields positive $J_{\mathbf{q}}^{12}$. Nevertheless, both approach yield maximum of the in-

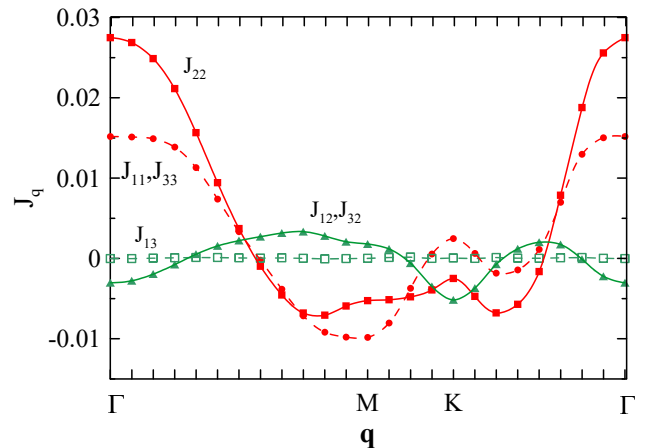


FIG. 10. (Color online) Real parts of the exchange interactions $J_{ij,\mathbf{q}}$ in trilayer system at $\beta = 18 \text{ eV}^{-1}$ in DFT+DMFT approach. The pairs of indexes ij at the exchange interactions correspond to the pairs of layers (1-bottom, 2-middle, 3-top layer)

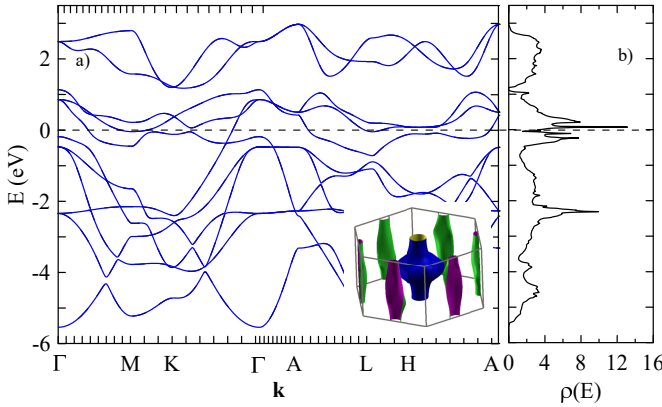


FIG. 11. (Color online) Band structure (a) and DFT density of states (b) of bulk CrTe₂ in paramagnetic phase. The inset in (a) shows the DFT Fermi surface.

terlayer exchange interaction at the Γ - M and Γ - K directions, which corresponds to the onset of incommensurate magnetic order between the layers. We note that to the best of our knowledge, at the moment there are no experimental data on bilayer systems available.

Let us consider what changes in DFT+DMFT results when adding one more layer in trilayer CrTe₂. The Fermi surface possesses an additional sheet near the Γ point (see Fig. 9). We find that the self-energies of trilayer system (not shown) are comparable to those of the bilayer one in Fig. 2. The maximum of the intralayer exchange interaction (see Fig. 10) shifts to the Γ point (instead of being in the near vicinity of the Γ point in bilayer system), which shows further stabilization of intralayer ferromagnetic order with increase of the number of layers. The exchange interaction between adjacent layers is negative (i.e. antiferromagnetic), similarly to the bilayer compound, with the maximum of the interlayer exchange interactions at the incommensurate positions in Γ - M and Γ - K directions.

To understand the effect of adding more layers in thick

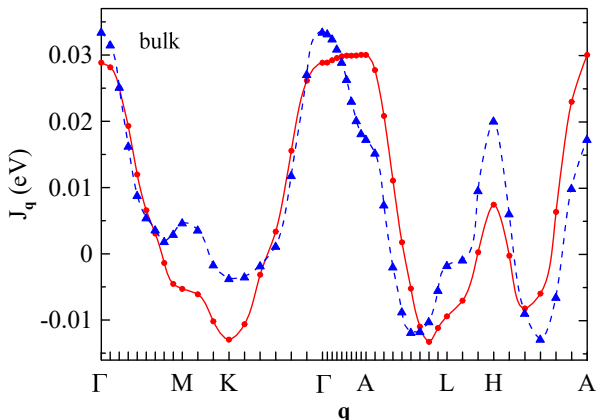


FIG. 12. (Color online) Exchange interaction in bulk CrTe₂ at $\beta = 24 \text{ eV}^{-1}$. The notations are the same as in Fig. 5.

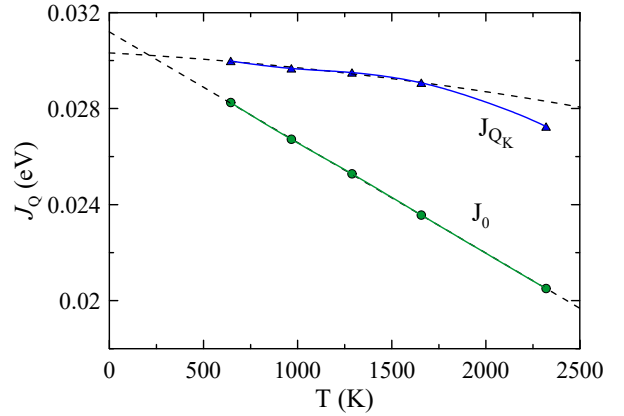


FIG. 13. (Color online) Temperature dependence of exchange interactions J_0 (circles) and J_{Q_K} (triangles) in bulk CrTe₂. Dashed lines show the result of extrapolation.

films, we consider bulk CrTe₂. The obtained band structure and Fermi surface (Fig. 11) reproduce those of previous study [7]. The Fermi surface sheet closest to the Γ point acquires the dispersion along k_z axis in agreement with the results for the trilayer system. The exchange interaction at $\beta = 24 \text{ eV}^{-1}$ (see Fig. 12) has local maximum at the Γ point, but its value at the A point of the Brillouin zone is somewhat larger than at Γ , showing the tendency to alternating orientation between the adjacent planes, similarly to that obtained for 2- and 3-layer system. However, with reducing temperature (see Fig. 13), we observe a clear tendency of changing the global maximum of exchange interaction to Γ point, which happens just at $T_C \simeq 250 \text{ K}$, comparable to the experimental Curie temperature. This implies formation of low temperature FM phase (in agreement with the experimental data), which changes upon heating to the state with long- or short-range antiferromagnetic order. We expect the long range antiferromagnetic order above T_C is destroyed by fluctuations. Therefore, we find an intriguing physical picture of competition of different types of magnetic correlations, which occurs just above the Curie temperature.

In view of the obtained results for the bilayer and trilayer systems, with decrease of the number of layers we expect the interlayer antiferromagnetic and incommensurate orders become progressively more favourable. Therefore, we expect the transition to interlayer incommensurate or antiferromagnetic states with decrease of the number of layers. In view of the delicate competition of various states, additional interactions, not included in the considered model (such as d - p and p - p interactions) may be important for obtaining critical number of layers for this transition, cf. Ref. [29].

IV. CONCLUSIONS

In summary, we have investigated magnetic properties of monolayer, bilayer, trilayer, and bulk CrTe₂. In

monolayer system in both, DFT and DFT+DMFT approaches we find preference for the incommensurate magnetic order with the wave vector \mathbf{Q}_K , which corresponds to 120° spin alignment. This order competes with AFM-zz magnetic order, earlier suggested for monolayer system.

In the bilayer and trilayer CrTe_2 in DFT+DMFT approach we find, in contrast to the DFT results, the tendency to the intralayer ferromagnetic order, which appear due to electronic correlations. At the same time, similarly to previous DFT+ U studies we find the tendency to the interlayer AFM order. This tendency is preserved at not too low temperatures in bulk CrTe_2 , and changes to FM order at low temperatures.

Most important result of the present study is the possibility of stabilization of intralayer FM order in CrTe_2 by correlations for number of layers bigger than one. Description of the transition from FM to AFM interlayer coupling with the decrease of the number of layers requires considering more sophisticated models, including non-local d - p (as well as p - p) interaction. The FM order in single-layer CrTe_2 , observed experimentally [11, 13, 14], requires further studies, and likely appears as an effect of substrate, cf. Ref. [16].

For future studies, account of full SU(2) Coulomb interaction, as well as the effect of the spin-orbit coupling would be desirable. Also, considering the effect of substrate, e.g., within the recently proposed approach of Ref. [46] is of certain interest.

ACKNOWLEDGEMENTS

We are grateful I. A. Goremykin for the help with using Quantum Espresso and Wannier90 packages and discussions, and to A. K. Nukhov for discussions of the obtained results. The paramagnetic DFT+DMFT calculations were supported by the Russian Science Foundation (Project No. 24-12-00186).

Appendix A: Single layer band structure in the ferromagnetic phase

In Fig. 14 we show band structure (cf. Refs. [13, 18]) and Fermi surfaces for the FM phase of single layer CrTe_2 . The nesting vectors \mathbf{q}_M and \mathbf{q}_K along $\Gamma - M$ and $\Gamma - K$ directions are close to the vectors $\mathbf{Q}_M = \pi(1, 1\sqrt{3})/a$ and \mathbf{Q}_K . By parameterizing the dispersion near the respective pairs of points of the Fermi surface by $e_{\mathbf{k}} = v_{F\sigma}\tilde{k}_x + \tilde{k}_y^2/(2m_{\sigma})$ where $\tilde{k}_{x,y}$ are local coordinates, assuming opposite Fermi velocities and masses of different spin states, we find at small temperatures the contribution to the exchange interactions

$$J_{\mathbf{q}} \propto \frac{\Delta^2}{|v_{F\uparrow}| + |v_{F\downarrow}|} \ln \frac{(|v_{F\uparrow}| + |v_{F\downarrow}|)^2}{|v_{F\uparrow}v_{F\downarrow}(\rho_{\uparrow} - \rho_{\downarrow})|} \quad (\text{A1})$$

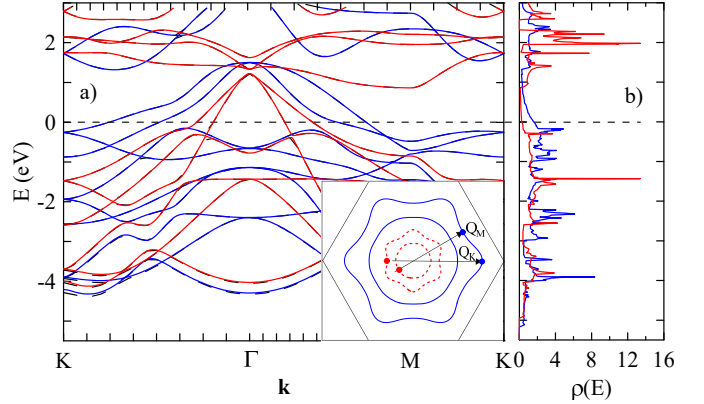


FIG. 14. (Color online) Band structure (a) and DFT density of states (b) of single-layer CrTe_2 in the FM phase. Blue (red) lines correspond to majority (minority) spin states. The inset in (a) shows the DFT Fermi surface. Points show parts of the Fermi surfaces connected by nesting vectors \mathbf{q}_M and \mathbf{q}_K ; the wave vectors \mathbf{Q}_M and \mathbf{Q}_K are shown for comparison.

where $\rho_{\sigma} = 1/|m_{\sigma}v_{F\sigma}|$ are the curvatures of the Fermi surface sheets, Δ is the average spin splitting. Although the Fermi velocities are somewhat different at the respective sheets of the Fermi surfaces, this does not prevent the nesting property, as far as the difference of curvatures $\rho_{\uparrow} - \rho_{\downarrow}$ remains small close to the considered points, connected by the vectors \mathbf{q}_M and \mathbf{q}_K .

Appendix B: Energy mapping

To estimate exchange interactions from the energies of various magnetic states, we perform calculations on the $2 \times 2\sqrt{3}$ supercell as shown on Fig. 15. We consider 4 different spin configurations to estimate exchange parameters. For all configurations the same lattice structure was used. Each atom has 6 nearest neighbours, 6 next nearest neighbours and 6 next to next nearest neighbours and we have 8 atoms in cell. To obtain corresponding energies it is enough to consider one of the atoms and multiply the result by 8 atoms.

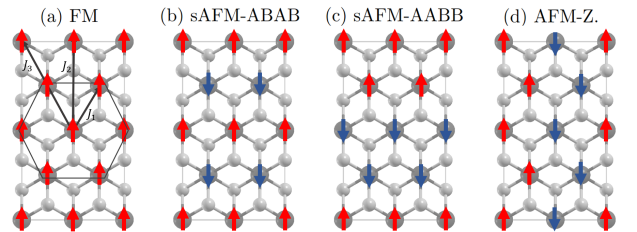


FIG. 15. (Color online) Schematic spin configuration for (a) FM (b) AFM-ABAB (c) AFM-AABB (d) AFM-zz.

The obtained DFT energies are

$$E_{\text{FM}} = E_0 - 24(J_1 + J_2 + J_3)S^2 = 128.968 \text{ eV}$$

$$E_{\text{AFM-ABAB}} = E_0 + 8(J_1 + J_2 - 3J_3)S^2 = 129.003 \text{ eV}$$

$$E_{\text{AFM-AABB}} = E_0 - 8(J_1 - J_2 - J_3)S^2 = 130.197 \text{ eV}$$

$$E_{\text{AFM-zz}} = E_0 - 8(J_2 - J_3)S^2 = 129.051 \text{ eV}$$

from which we get exchange parameters, presented in Table I.

[1] B. Shabbir, M. Nadeem, Z. Dai, M. S. Fuhrer, Q.-K. Xue, X. Wang, and Q. Bao, Long range intrinsic ferromagnetism in two dimensional materials and dissipationless future technologies, *Appl. Phys. Rev.* **5**, 041105 (2018).

[2] H. Li, S. Ruan, and Y.-J. Zeng, Intrinsic Van der Waals magnetic materials from bulk to the 2D limit: new frontiers of spintronics, *Adv. Mater.* **31**, 1900065 (2019).

[3] N. Sethulakshmi, A. Mishra, P.M. Ajayan, Y. Kawazoe, A. K. Roy, A. K. Singh, C. S. Tiwary, Magnetism in two-dimensional materials beyond graphene, *Mater. Today*, **27**, 107 (2019).

[4] X. Jiang, Q. Liu, J. Xing, N. Liu, Y. Guo, Z. Liu, J. Zhao, Recent progress on 2D magnets: Fundamental mechanism, structural design and modification, *Appl. Phys. Rev.* **8**, 031305 (2021).

[5] Z. Liu, L. Deng, and B. Peng, Ferromagnetic and ferroelectric two-dimensional materials for memory application, *Nano Research* **14**, 1802 (2021).

[6] Y. Yao, X. Zhan, M. G. Sendeku, P. Yu, F. T. Dajan, C. Zhu, N. Li, J. Wang, F. Wang, Z. Wang, and J. He, Recent progress on emergent two-dimensional magnets and heterostructures, *Nanotechnology* **32** 472001 (2021).

[7] D. C. Freitas, R. Weht, A. Sulpice, G. Remenyi, P. Strobel, F. Gay, J. Marcus, and M. Núñez-Regueiro, Ferromagnetism in layered metastable 1T-CrTe₂, *Journ. Phys.: Cond. Mat.* **27** 176002 (2015).

[8] A. Purbawati, J. Coraux, J. Vogel, A. Hadj-Azzem, N. Wu, N. Bendiab, D. Jegouso, J. Renard, L. Marty, V. Bouchiat, A. Sulpice, L. Aballe, M. Foerster, F. Genuzio, A. Locatelli, T. O. Menteş, Z. V. Han, X. Sun, M. Núñez-Regueiro, and N. Rougemaille, In-plane magnetic domains and Néel-like domain walls in thin flakes of the room temperature CrTe₂ Van der Waals ferromagnet, *ACS Applied Materials & Interfaces* **12** 30702 (2020).

[9] F. Fabre, A. Finco, A. Purbawati, A. Hadj-Azzem, N. Rougemaille, J. Coraux, I. Philip, and V. Jacques, Characterization of room-temperature in-plane magnetization in thin flakes of CrTe₂ with a single-spin magnetometer, *Phys. Rev. Materials* **5** 034008 (2021).

[10] X. Sun, W. Li, X. Wang, Q. Sui, T. Zhang, Z. Wang, L. Liu, D. Li, S. Feng, S. Zhong, H. Wang, V. Bouchiat, M. Nunez Regueiro, N. Rougemaille, J. Coraux, A. Purbawati, A. Hadj-Azzem, Z. Wang, B. Dong, X. Wu, T. Yang, G. Yu, B. Wang, Z. Han, X. Han, and Z. Zhang, Room temperature ferromagnetism in ultra-thin Van der Waals crystals of 1T-CrTe₂, *Nano Research* **13** 3358 (2020).

[11] L. Meng, Z. Zhou, M. Xu, S. Yang, K. Si, L. Liu, X. Wang, H. Jiang, B. Li, P. Qin, P. Zhang, J. Wang, Z. Liu, P. Tang, Y. Ye, W. Zhou, L. Bao, H.-J. Gao, and Y. Gong, Anomalous thickness dependence of Curie temperature in air-stable two-dimensional ferromagnetic 1T-CrTe₂ grown by chemical vapor deposition, *Nature Communications* **12** 809 (2021).

[12] Y. Sun, P. Yan, J. Ning, X. Zhang, Y. Zhao, Q. Gao, M. Kanagaraj, K. Zhang, J. Li, X. Lu, Y. Yan, Y. Li, Y. Xu, and L. He, Ferromagnetism in two-dimensional CrTe₂ epitaxial films down to a few atomic layers, *AIP Advances* **11** 035138 (2021).

[13] X. Zhang, Q. Lu, W. Liu, W. Niu, J. Sun, J. Cook, M. Vaninger, P. Miceli, D. Singh, S.-W. Lian, T.-R. Chang, X. He, J. Du, L. He, G. Bian, and Y. Xu, Room-temperature intrinsic ferromagnetism in epitaxial CrTe₂ ultrathin films, *Nature Communications* **12** 2492 (2021).

[14] X. Liu, P. Huang, Y. Xia, L. Gao, L. Liao, B. Cui, D. Backes, G. van der Laan, T. Hesjedal, Y. Ji, P. Chen, Y. Zhang, F. Wu, M. Wang, J. Zhang, G. Yu, C. Song, Y. Chen, Z. Liu, Y. Yang, Y. Peng, G. Li, Q. Yao, and X. Kou, Wafer-scale epitaxial growth of the thickness-controllable Van der Waals ferromagnet CrTe₂ for reliable magnetic memory applications, *Advanced Functional Materials* **33** 2304454 (2023).

[15] H. Zheng, C. Huang, F. Lin, J. Fan, H. Liu, L. Zhang, C. Ma, C. Wang, Y. Zhu, and H. Yang, Two-dimensional van der Waals ferromagnetic thin film CrTe₂ with high Curie temperature and metallic conductivity, *Appl. Phys. Lett.* **122** 023103 (2023).

[16] D. Wang, X. Wang, B. Hu, J. Wang, Y. Zou, J. Guo, Z. Li, S. Wang, Y. Li, G. Song, H. Wang, and Y. Liu, Strain- and electron doping-induced in-plane spin orientation at room temperature in single-layer CrTe₂, *ACS Applied Materials & Interfaces* **16** 28791 (2024).

[17] J.-J. Xian, C. Wang, J.-H. Nie, R. Li, M. Han, J. Lin, W.-H. Zhang, Z.-Y. Liu, Z.-M. Zhang, M.-P. Miao, Y. Yi, S. Wu, X. Chen, J. Han, Z. Xia, W. Ji, and Y.-S. Fu, Spin mapping of intralayer antiferromagnetism and field-induced spin reorientation in monolayer CrTe₂, *Nature Communications* **13** 257 (2022).

[18] S. Li, S.-S. Wang, B. Tai, W. Wu, B. Xiang, X.-L. Sheng, and S. A. Yang, Tunable anomalous Hall transport in bulk and two-dimensional 1T - CrTe₂: A first-principles study, *Phys. Rev. B* **103** 045114 (2021).

[19] Y. Liu, S. Kwon, G. J. de Coster, R. K. Lake, and M. R. Neupane, Structural, electronic, and magnetic properties of CrTe₂, *Phys. Rev. Materials* **6** 084004 (2022).

[20] X. Yang, X. Zhou, W. Feng, and Y. Yao, Tunable magneto-optical effect, anomalous Hall effect, and anomalous Nernst effect in the two-dimensional room-temperature ferromagnet 1T CrTe₂, *Phys. Rev. B* **103** 024436 (2021).

[21] M. Yao, J. Pan, W. Xie, Z. Yang, M. Li, and H. Wang,

Control of the magnetic anisotropy and Curie temperature of monolayer 1T-CrTe₂ for room temperature application, *Appl. Phys. Lett.* **123**, 242405 (2023)

[22] H. Y. Lv, W. J. Lu, D. F. Shao, Y. Liu, and Y. P. Sun, Strain-controlled switch between ferromagnetism and antiferromagnetism in 1T-CrX₂ (X = Se, Te) monolayers, *Phys. Rev. B* **92**, 214419 (2015)

[23] P. Gao, X. Li, and J. Yang, Thickness dependent magnetic transition in few layer 1T phase CrTe₂, *J. Phys. Chem. Lett.* **12**, 6847 (2021).

[24] A. Elrashidy and J.-A. Yan, Magnetic stability, fermi surface topology, and spin-correlated dielectric response in monolayer 1T-CrTe₂, *ArXiv:2310.19735*.

[25] N. Abuawwad, M. Dos Santos Dias, H. Abusara, and S. Lounis, Noncollinear magnetism in two-dimensional CrTe₂, *Journ. Phys.: Cond. Matt.* **34**, 454001 (2022)

[26] A. Otero Fumega, J. Phillips, and V. Pardo, Controlled two-dimensional ferromagnetism in 1T-CrTe₂: The role of charge density wave and strain, *The Journal of Phys. Chemistry C* **124**, 21047 (2020)

[27] L. Wu, L. Zhou, X. Zhou, C. Wang, and W. Ji, In-plane epitaxy-strain-tuning intralayer and interlayer magnetic coupling in CrSe₂ and CrTe₂ monolayers and bilayers, *Phys. Rev. B* **106**, L081401 (2022)

[28] H. Zhu, Y. Gao, Y. Hou, Z. Gui, and L. Huang, Insight into strain and electronic correlation dependent magnetism in monolayer 1T-CrTe₂, *Phys. Rev. B* **108**, 144404 (2023)

[29] C. Wang, X. Zhou, L. Zhou, Y. Pan, Z.-Y. Lu, X. Wan, X. Wang, and Wei Ji, Bethe-Slater-curve-like behavior and interlayer spin-exchange coupling mechanisms in two-dimensional magnetic bilayers, *Phys. Rev. B* **102**, 020402(R) (2020)

[30] A. A. Katanin, A. S. Belozerov, A. I. Lichtenstein, M. I. Katsnelson, Exchange interactions in iron and nickel: DFT+DMFT study in paramagnetic phase, *Phys. Rev. B* **107**, 235118 (2023).

[31] P. Giannozzi, et. al., Quantum ESPRESSO: a modular and open-source software project for quantum simulations of materials, *J. Phys.: Condens. Matter* **21**, 395502 (2009); Advanced capabilities for materials modelling with Quantum ESPRESSO, *ibid.* **29**, 465901 (2017); <https://www.quantum-espresso.org>.

[32] G. Prandini, A. Marrazzo, I. E. Castelli, N. Mounet, and N. Marzari, Precision and efficiency in solid-state pseudopotential calculations, *Computational Materials* **4**, 72 (2018); <http://materialscloud.org/sssp>

[33] R. Sakuma, Symmetry-adapted Wannier functions in the maximal localization procedure, *Phys. Rev. B* **87**, 235109 (2013).

[34] G. Pizzi, et. al., Wannier90 as a community code: new features and applications, *J. Phys. Cond. Matt.* **32**, 165902 (2020); <http://www.wannier.org>.

[35] A. N. Rubtsov, V. V. Savkin, and A. I. Lichtenstein, Continuous-time quantum Monte Carlo method for fermions, *Phys. Rev. B* **72**, 035122 (2005); P. Werner, A. Comanac, L. de Medici, M. Troyer, and A. J. Millis, Continuous-Time Solver for Quantum Impurity Models, *Phys. Rev. Lett.* **97**, 076405 (2006).

[36] Li Huang, Y. Wang, Zi Yang Meng, L. Du, P. Werner, and Xi Dai, iQIST: An open source continuous-time quantum Monte Carlo impurity solver toolkit, *Comp. Phys. Comm.* **195**, 140 (2015); Li Huang, iQIST v0.7: An open source continuous-time quantum Monte Carlo impurity solver toolkit, *Comp. Phys. Comm.* **221**, 423 (2017).

[37] V. I. Anisimov, F. Aryasetiawan, and A. I. Lichtenstein, *J. Phys.: Condens. Matter* **9**, 767 (1997)

[38] M. T. Czyzyk and G. A. Sawatzky, Local-density functional and on-site correlations: The electronic structure of La₂CuO₄ and LaCuO₃, *Phys. Rev. B* **49**, 14211 (1994).

[39] A. I. Liechtenstein, M. I. Katsnelson, V. P. Antropov, and V. A. Gubanov, Local spin density functional approach to the theory of exchange interactions in ferromagnetic metals and alloys, *Journal of Magnetism and Magnetic Materials* **67**, 65 (1987)

[40] D. M. Korotin, V. V. Mazurenko, V. I. Anisimov, and S. V. Streltsov, Calculation of exchange constants of the Heisenberg model in plane-wave-based methods using the Green's function approach, *Phys. Rev. B* **91**, 224405 (2015)

[41] Package used for calculations is posted on [GitHub](https://github.com).

[42] A. A. Katanin, DFT+DMFT study of exchange interactions in cobalt and their implications for the competition of hcp and fcc phases, *Phys. Rev. B* **108**, 235170 (2023).

[43] E. M. Agapov, I. A. Kruglov, A. A. Katanin, MXene Fe₂C as a promising candidate for the 2D XY ferromagnet, *2D Mater.* **11**, 025001 (2024).

[44] G. Rohringer, H. Hafermann, A. Toschi, A. A. Katanin, A. E. Antipov, M. I. Katsnelson, A. I. Lichtenstein, A. N. Rubtsov, K. Held, Diagrammatic routes to nonlocal correlations beyond dynamical mean field theory, *Rev. Mod. Phys.* **90**, 025003 (2018).

[45] A. A. Katanin, Generalized dynamical mean-field theory of two-sublattice systems with long-range interactions and its application to study charge and spin correlations in graphene, *Phys. Rev. B* **104**, 245142 (2021); Charge and spin correlations in insulating and incoherent metal states of twisted bilayer graphene, *Phys. Rev. B* **106**, 115147 (2022).

[46] A. Mazitov, I. Kruglov, A. V. Yanilkin, A. V. Arsenin, V. S. Volkov, D. G. Kvashnin, A. R. Oganov, K. S. Novoselov, Substrate-aware computational design of two-dimensional materials, *ArXiv: 2408.08663*.